Vol. 60 No 04 (236) 2020
DOI: https://doi.org/10.5564/pmas.v60i4.1501
PMAS
Proceedings of the Mongolian Academy of Sciences

ARTICLE

Finding a suitable fit function used to determine the Physical width of the Flux tube with Dynamical fermions

Battogtokh Purev*, Sodbileg Chagdaa and Enkhtuya Galsandorj

Department of Theoretical and High Energy Physics, Institute of Physics and Technology, Mongolian Academy of Sciences, Ulaanbaatar, Mongolia

ARTICLE INFO: Received: 19 Aug, 2020; Accepted: 29 Nov, 2020

Abstract: *We have determined the width of the flux tube for several temperatures and distances using four different fit functions in order to determine the appropriate function that fits the data of the middle transverse distribution of flux tube with the dynamical fermions. Our results have revealed that only one fitting function cannot determine the width of the flux tube at the given temperatures and distances. We conclude that appropriate fit functions are a four coefficient function where R < 0.8 fm and where Gaussian function is R > 0.8 fm.*

Keywords: *lattice QCD; dynamical fermions; width of the flux tube;*

INTRODUCTION

In the previous study [1], we measured the flux tube with dynamical quarks configurations in full QCD with (2+1) flavors using HISQ/tree action on the lattice of volume 32^3 x 12 at different temperatures and distances as part of the research to study the mechanism of color confinement and the structure of the hadron. At the end of 2019, we increased the statistics for this measurement. Using this increased data, we can find an appropriate fit function to determine the width of the flux tube with dynamical fermions. Computing the width of the flux tube is an important part of the study of the mechanism of confinement. Therefore, this work will give us better chances to improve our understanding of the mechanism of confinement.

Computation of the width of the flux tube

The flux tube between quark and anti-quark is extracted from the correlation of the plaquette with the Polyakov loops. From ref. [2], we can see that the correlation function can express squared components of the chromo-electric ($\boldsymbol{E^2}$) and chromo-magnetic ($\boldsymbol{B^2}$) field distributions. The physical flux tube is defined by a spatial distribution of energy density via

$$\varepsilon = \boldsymbol{E^2} + \boldsymbol{B^2}. \qquad (1)$$

A two-dimensional image of the flux tube is illustrated in Figure 1.

***corresponding author: pbattogtokh@gmail.com** **https://orcid.org/0000-0002-5170-1267**

PMAS
Proceedings of the Mongolian Academy of Sciences
Vol. 60 No 04 (236) 2020
DOI: https://doi.org/10.5564/pmas.v60i4.1501

One can easily show that the longitudinal and the transverse directions of the distributions are respectively denoted by ($x_{\parallel}$) and ($x_{\perp}$), and the horizontal red line represents the mediator plane between quark and anti-quark.

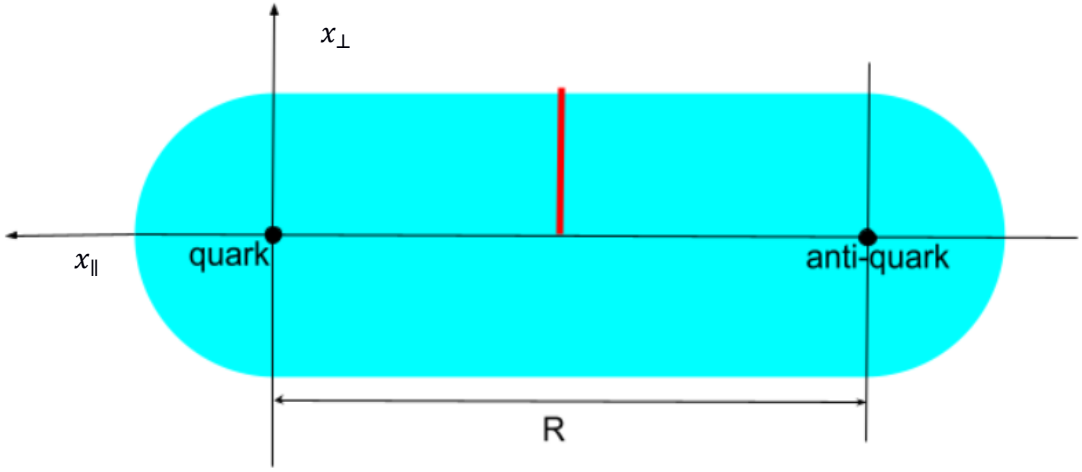

Figure 1. 2D projection of the flux tube

To compute the physical width of the flux tube, we fit the energy density data in mediator plane with appropriate fit function, $F(x_{\perp})$. There are many kinds of fitting techniques and functions used in previous studies [3-6]. We here present the technique and function that is consistent with our middle transverse energy density data. However, constant-coefficient k was added to the fit functions because our simulation used the reference point method to reduce the statistical noise. After the fit, the appropriate fit function will be selected by the chi-square X^2 values.

Following which, with our fit, we calculate other quantitative parameters using the fitting coefficients, considering the normalized fit function, $F(x_{\perp})$-k, as an energy density data, the root mean square width of the flux tube [3],

$$\frac{D_{\varepsilon}^2}{a^2} = \frac{\int_{-\infty}^{+\infty} x_{\perp}^2 (F(x_{\perp}) - k) d^2 x_{\perp}}{\int_{-\infty}^{+\infty} (F(x_{\perp}) - k) d^2 x_{\perp}}, \qquad (2)$$

where a is lattice spacing.

Fitting techniques are commonly used in lattice gauge theory and particularly, in computing the width of the flux tube. There are several conventional fit functions [3-5] that are applied for determining the width in overall conditions. In our case this is the first time computing the width of the flux tube with dynamical fermions after using it to calculate the pure gauge flux tube. Therefore, we had to try all these functions and choose one of them. Let us now have a look into these functions and their fit result for our data.

Exponential fit function

Initially, we fitted the middle transverse data of the energy density with the normalized exponential fit function proposed in Ref. [3],

$$F(x_{\perp}) = a_1 e^{-b_1 x_{\perp}} + k_1, \qquad (3)$$

Where a_1, b_1 and k_1 are fitting coefficients. We can easily imagine that the equation is exponentially deceased from $k_1 + a_1$ to the k_1 at a positive range.

Now let's analytically calculate the width of the flux tube from equation (2) using this fit function equation (3). The width is expressed by the fitting coefficient,

$$\frac{D_{\varepsilon}^2}{a^2} = \frac{6}{b_1^2}. \qquad (4)$$

Table 1 shows the result of the exponential fitting in a lattice spacing unit.

PMAS
Proceedings of the Mongolian Academy of Sciences
Vol. 60 No 04 (236) 2020
DOI: https://doi.org/10.5564/pmas.v60i4.1501

Table 1. The fitting results of the Equation (3) and the square root width equation (4) in a lattice unit.

β	R/a	a_1	b_1	k_1	$\sqrt{\chi^2}$	D_ε^2/a^2
6.39	4	0.00484(16)	0.8201(367)	0.00024(2)	1.28	8.92(80)
	6	0.00110(14)	0.2670(710)	0.00026(8)	1.36	84.14(44.54)
	8	0.00075(35)	0.4151(2340)	0.00101(6)	3.49	34.83(39.27)
	10	0.00054(33)	1.521(1.341)	0.00160(3)	2.97	2.59(4.57)
	12	-0.00084(20)	1.781(727)	0.00005(2)	0.69	1.89(1.54)
	14	0.00065(17)	1.243(725)	0.00034(2)	0.55	3.88(4.53)
	16	0.00078(19)	0.6794(2398)	0.00012(4)	1.61	13.00(9.18)
6.423	4	0.00441(19)	0.9096(362)	-0.00024(1)	1.49	7.25(58)
	6	0.00123(13)	0.4032(616)	0.00043(3)	1.07	36.91(11.29)
	8	0.00039(31)	0.6073(4118)	0.00016(2)	1.83	16.27(22.07)
	10	0.0003(17)	1.858(955)	0.00029(1)	1.02	1.74(1.79)
	14	0.00020(7)	0.3852(2303)	0.00082(2)	0.72	40.44(48.35)
6.445	4	0.00387(11)	0.7779(311)	0.00020(2)	2.12	9.91(79)
	6	0.00077(6)	0.2161(505)	0.00076(6)	1.00	128.5(60.1)
	10	0.00005(13)	0.609(1.755)	0.00077(2)	1.02	16.19(93.40)
	12	-0.00027(17)	1.28(1.17)	0.00001(2)	1.50	3.67(6.71)
	14	0.00024(14)	3.45(13.82)	0.00018(1)	1.13	0.504(4.035)
	16	0.00030(7)	1.84(1.19)	0.00021(1)	0.55	1.78(2.31)
6.474	4	0.00324(3)	0.7188(194)	0.00076(1)	2.28	11.61(63)
	6	0.00065(4)	0.3768(409)	0.00035(1)	0.78	42.26(9.17)
	8	0.00039(9)	0.4528(1323)	0.00032(2)	1.93	29.27(17.10)
	12	-0.00029(11)	3.80(13.98)	0.00042(1)	1.90	0.415(3.055)
	14	0.00017(8)	0.4312(2541)	0.00013(1)	1.57	32.27(38.03)
	16	0.00019(4)	0.2097(1304)	0.00016(4)	0.89	136.4(169.6)
6.5	4	0.00295(3)	0.6789(188)	0.00052(1)	1.39	13.02(72)
	6	0.00083(5)	0.3909(376)	0.00013(1)	1.14	39.28(7.57)
	8	0.00045(9)	0.7585(1824)	0.00046(1)	1.24	10.43(5.02)
	10	0.00016(3)	0.2811(995)	0.00016(1)	1.20	75.93(53.76)
	12	-0.00004(8)	0.658(1.399)	0.00020(1)	2.10	13.86(58.96)
	14	0.00016(3)	0.3180(1444)	0.00046(1)	0.92	59.34(53.90)

Gaussian fit function

During the exponential fit, we observed that the sharp decrease of the exponential fitting curve in the region close to zero on the $x_\perp$-axis contradicts most of our data. The data looks like one side of a bell in this region. Therefore, we needed to choose another fit function that would have shape of a bell curve, such as the Gaussian function.

Accordingly, our second fit function is defined in Ref. [4] with the additional coefficient,

$$F(x_\perp) = a_2\, e^{-b_2 x_\perp^2} + k_2. \qquad (5)$$

From the equation (2), its width is given by

$$\frac{D_\varepsilon^2}{a^2} = \frac{1}{b_2}. \qquad (6)$$

We have displayed its fitting results in Table 2.

Vol. 60 No 04 (236) 2020
DOI: https://doi.org/10.5564/pmas.v60i4.1501

Table2. The fitting results of equation (5) and the square root width of equation (6) in a lattice unit.

β	R/a	a_2	b_2	k_2	$\sqrt{\chi^2}$	D_ε^2/a^2
6.39	4	0.00434(16)	0.4549(303)	0.00030(2)	1.34	2.198(146)
	6	0.00072(11)	0.0522(153)	0.00035(1)	1.45	19.15(5.62)
	8	0.00048(16)	0.0766(408)	0.00102(4)	3.40	13.05(6.94)
	10	0.00054(33)	1.243(1.186)	0.00161(3)	2.96	0.805(768)
	12	-0.00084(20)	1.163(438)	0.00005(2)	0.68	0.860(324)
	14	0.00063(16)	0.6109(3978)	0.00034(2)	0.54	1.637(1.066)
	16	0.00075(16)	0.2218(938)	0.00013(3)	1.51	4.509(1.907)
6.423	4	0.00363(19)	0.4402(288)	-0.00023(1)	1.72	2.27(15)
	6	0.00097(9)	0.1114(189)	0.00047(2)	1.01	8.98(1.52)
	8	0.00034(18)	0.1452(928)	0.00016(2)	1.77	6.89(4.40)
	10	0.00030(16)	0.5065(4970)	0.00029(1)	1.60	1.97(1.94)
	12	0.00008(8)	0.0152(411)	0.00059(9)	2.23	65.9(178.5)
	14	0.00020(7)	0.2581(1784)	0.00083(1)	0.72	3.88(2.68)
6.445	4	0.00349(9)	0.4866(223)	0.00025(1)	1.80	2.55(9)
	6	0.00058(4)	0.0526(84)	0.00086(2)	0.88	19.02(3.04)
	8	0.00036(13)	0.0095(65)	0.00049(14)	0.32	105.1(72.0)
	12	-0.00024(15)	0.6570(7391)	0.00007(1)	1.50	1.52(1.71)
	14	-0.00024(14)	2.914(8.404)	0.00018(1)	1.13	0.343(990)
	16	0.00030(7)	1.2512(7424)	0.00021(1)	0.55	0.799(474)
6.474	4	0.00316(3)	0.4938(214)	0.00082(1)	2.87	2.025(88)
	6	0.00051(4)	0.1238(195)	0.00038(9)	0.95	19.02(3.04)
	8	0.00032(7)	0.1220(380)	0.00033(10)	1.87	8.20(2.55)
	12	-0.00029(11)	2.49(3.90)	0.00042(1)	1.91	0.4023(6307)
	14	0.00011(5)	0.0740(484)	0.00013(1)	1.55	13.51(8.83)
	16	0.00020(7)	1.091(779)	0.00020(1)	1.00	0.7992(4742)
6.5	4	0.00282(4)	0.4824(197)	0.00057(1)	1.60	2.073(85)
	6	0.00068(4)	0.1219(125)	0.00017(1)	1.05	8.203(841)
	8	0.00044(9)	0.4358(1438)	0.00047(1)	1.19	2.294(757)
	10	0.00011(2)	0.0506(182)	0.00017(1)	1.22	19.75(7.10)
	12	-0.00003(9)	1.11(6.82)	0.00019(1)	2.11	0.90(5.58)
	14	0.00010(2)	0.0608(280)	0.00047(1)	0.92	16.45(7.57)

Coulombic fit function

Another function that can represent this bell curve is Coulomb function [3],

$$F(x_\perp) = \frac{a_3}{(b_3+x_\perp^2)^3} + k_3, \qquad (7)$$

where k_3 is added coefficient, because of the reference point method. Its widths are computed via the integral method from the equation (2),

$$\frac{D_\varepsilon^2}{a^2} = b_3. \qquad (8)$$

Also, its results are tabulated in Table 3.

Table3. Fitting results of equation (7) and square root width of equation (8)

β	R/a	a_3	b_3	k_3	$\sqrt{\chi^2}$	D_ε^2/a^2
6.39	4	0.59(10)	5.06(31)	0.000280(17)	1.11	5.06(31)
	6	65(65)	43.17(15.28)	0.000330(44)	1.42	43.17(15.28)
	8	17(35)	32.77(24.72)	0.001010(48)	3.44	32.77(24.72)
	10	0.0034(113)	1.85(2.19)	0.00160(3)	2.97	1.85(2.19)
	12	0.0041(216)	1.70(87)	0.000055(19)	0.69	1.70(87)
	14	0.0216(469)	3.23(2.42)	0.000340(22)	0.54	3.23(2.42)
	16	0.92(1.34)	10.73(5.59)	0.000120(35)	1.54	10.73(5.59)
6.423	4	0.43(7)	4.77(29)	-0.000240(11)	1.37	4.77(29)
	6	9.63(5.39)	21.10(4.32)	0.000460(18)	1.00	21.10(4.32)
	8	1.21(2.81)	15.52(14.37)	0.000160(20)	1.80	15.52(14.37)
	10	0.02(6)	3.91(4.46)	0.000290(13)	1.61	3.91(4.46)

Vol. 60 No 04 (236) 2020
DOI: https://doi.org/10.5564/pmas.v60i4.1501

	12	72.2(708.5)	103(332)	0.000600(57)	2.24	103(332)
	14	0.23(51)	10.36(8.31)	0.000830(14)	0.72	10.36(8.31)
	16	-24(183)	66(167)	0.000610(45)	1.34	66(167)
6.445	4	0.44(5)	4.97(20)	0.00023(1)	1.42	4.97(20)
	6	67.34(40.61)	47.9(9.79)	0.00084(2)	0.89	47.9(9.8)
	8	12387(31760)	316.1(233.1)	0.00045(16)	0.32	316(233)
	10	0.151(905)	12.36(28.05)	0.00077(1)	1.01	12.4(28.0)
	12	-0.006(21)	2.82(3.65)	0.00001(15)	1.50	2.82(3.65)
	14	-0.0002(15)	0.96(2.37)	0.00018(1)	1.13	0.96(2.37)
	16	0.0011(26)	1.54(1.23)	0.00021(1)	0.55	1.54(1.23)
6.474	4	0.41(4)	5.07(17)	0.00080(1)	2.00	5.07(17)
	6	3.76(1.75)	18.94(3.20)	0.00037(1)	0.87	18.94(3.20)
	8	2.24(2.39)	18.80(7.47)	0.00033(1)	1.88	18.80(7.47)
	10	3506(11350)	253(241)	0.00052(10)	1.03	253(241)
	12	64585(416000)	670(1190)	0.00025(26)	1.67	670(1190)
	14	2.44(5.56)	26.90(22.70)	0.00013(1)	1.56	26.90(22.70)
	16	32.11(62.54)	61.95(40.99)	0.00017(1)	0.90	61.95(40.99)
6.5	4	0.42(4)	5.28(15)	0.00056(1)	1.03	5.28(0.15)
	6	5.74(1.90)	20.03(2.38)	0.00015(1)	1.02	20.03(2.38)
	8	0.08(8)	5.66(2.14)	0.00047(1)	1.20	5.66(2.14)
	10	11.31(13.94)	45.26(19.72)	0.00017(1)	1.22	45.26(19.72)
	12	-0.10(77)	14.57(41.43)	0.00020(1)	2.10	14.57(41.43)
	14	4.92(7.97)	34.90(19.99)	0.00047(1)	0.92	34.90(19.99)
	16	29964(1170000)	798(8363)	0.00010(46)	1.11	798(8363)

Four coefficient exponential fit function

Although the bell-shaped curves have characterized most of our data, a few parts of these data are better described by the exponential decreasing curves. Previously, we determined three different functions that one can express one of the two types of curves separately. Now let us try to describe the new function that illustrates both curves. It is our fourth fitting function which is given in Ref. [5],

$$F(x_\perp) = F_0 \exp\left(\frac{2}{\lambda}\sqrt{x_\perp^2 - v^2} + \frac{2v}{\lambda}\right) + k_4. \quad (9)$$

This function has four fitting coefficients, so let us call it the four coefficient fit function. After which, the square root of the width is computed through the integral method (1),

$$\frac{D_\varepsilon^2}{a^2} = \frac{3}{2}\lambda^2 + 2\frac{\lambda v^2}{\lambda + 2v}. \quad (10)$$

The fitting coefficients and the widths are shown in Table 4.

Table4. Fitting results of equation (9) and square root width of equation (10)

β	R/a	F_0	λ	v	k4	$\sqrt{\chi^2}$	D_ε^2/a²
6.39	4	0.068(1)	1.68(19)	0.7091(2098)	0.00027(2)	1.08	4.79(1.24)
	6	-0.034(8)	6.38(2.11)	-0.0005(9796)	0.00030(7)	1.37	61.00(40.33)
	8	-0.022(6)	0.76(20.14)	16.6(455.3)	0.00102(5)	3.44	1.2(712.1)
	10	0.023(7)	0.23(10.36)	3.4(156.8)	0.00161(3)	2.99	0.83(76.02)
	16	0.028(3)	0.31(13.68)	14.1(635.7)	0.00013(3)	1.53	4.4(397.6)
6.423	4	0.646(1)	1.68(15)	0.558(185)	-0.00024(1)	1.33	4.69(98)
	6	0.032(2)	1.72(1.99)	4.59(6.92)	0.00047(2)	1.01	11.07(28.31)
	8	0.09(31.38)	1.67(5.97)	-3.25(18.37)	0.00016(2)	1.80	3.12(21.85)
	10	0.017(5)	0.38(9.73)	4.9(132.3)	0.00029(1)	1.62	2.02(105.8)
	14	0.014(3)	0.29(19.12)	12.9(855.3)	0.00083(1)	0.72	3.9(510.6)
6.445	4	0.060(6)	1.55(15)	0.874(174)	0.00023(1)	1.39	4.30(96)
	10	0.0096(64)	1.1(16.0)	3.9(67.0)	0.00077(1)	1.02	5.6(176.5)
	16	0.017(2)	0.29(5.34)	2.6(52.7)	0.00021(1)	0.55	0.83(32.15)
6.474	4	0.0566(2)	1.97(12)	0.533(93)	0.00078(1)	1.68	6.20(83)
	6	0.025(1)	5.13(84)	0.104(423)	0.00035(1)	0.79	39.50(13.02)
	16	0.014(2)	5.66(3.39)	0.004(1.459)	0.00018(2)	0.90	47.97(57.57)

Vol. 60 No 04 (236) 2020
DOI: https://doi.org/10.5564/pmas.v60i4.1501

6.5	4	0.0537(2)	1.99(9)	0.597(72)	0.00055(1)	0.77	6.37(67)
	10	0.021(4)	6.94(3.54)	-0.029(1.452)	0.00017(2)	1.21	72.28(73.51)
	14	0.015(17)	5.40(4.23)	-0.747(2.939)	0.00047(2)	0.92	45.36(53.61)

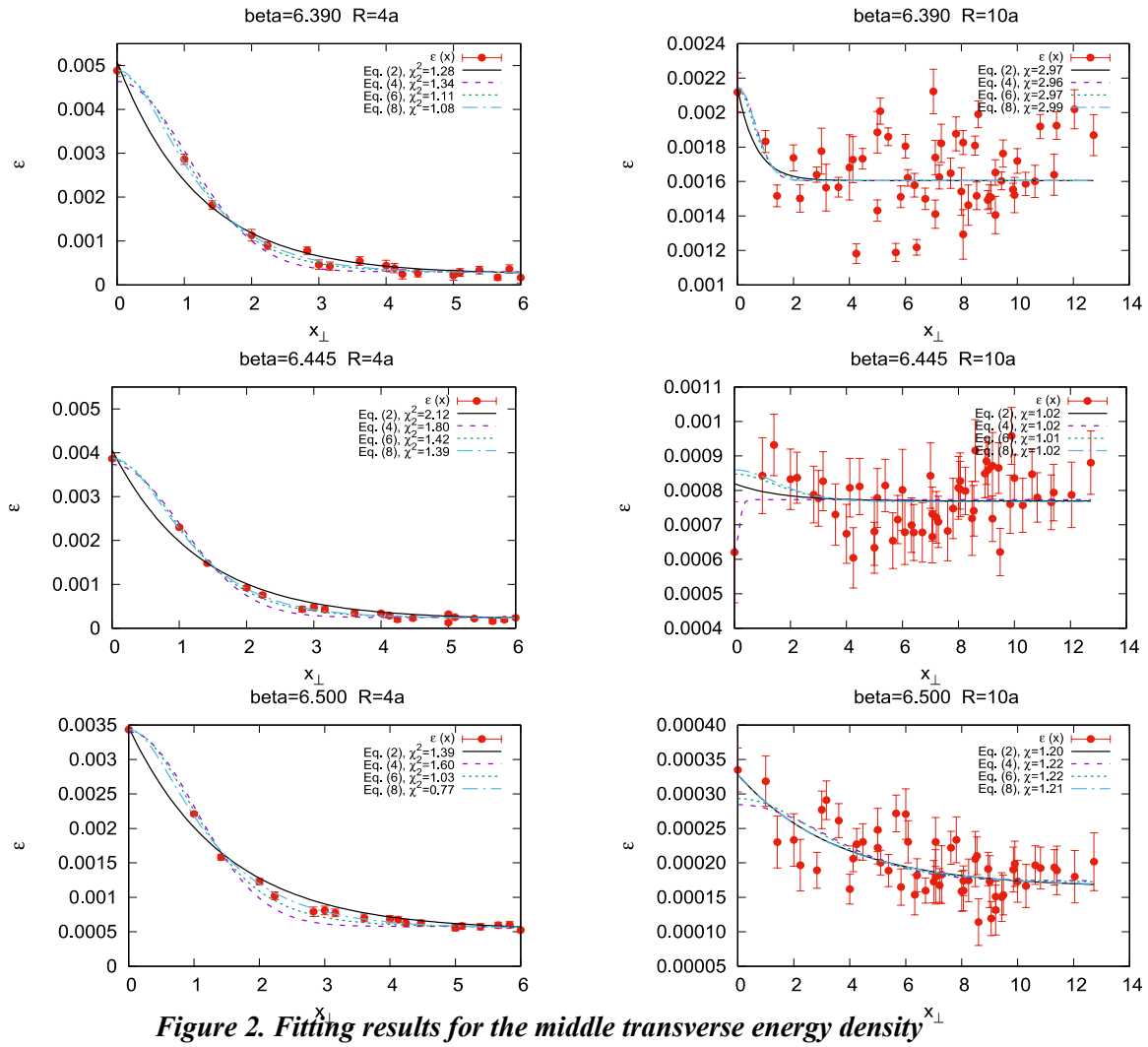

Figure 2. Fitting results for the middle transverse energy density at different distances and temperatures

RESULTS AND DISCUSSION

In this work, we have determined the width of the flux tube in full QCD with dynamical fermions using four fit functions. The flux tube is measured by dynamical fermion configurations on the lattice of volume 32^3x8 for five different temperatures T/Tc = 0.97, 1.00, 1.03, 1.06 and 1.09, and seven distances R/a = 4, 6, 8, 10, 12, 14 and 16 respectively. The gradient flow method [7, 8] suppressed the static noise of the configurations at the flow time t=0.25. Tables 1-4 present the width-values in the lattice unit.

We have plotted the transverse distribution of the energy density in the mediator plane and their fitting curves were drawn by the fit functions at several temperatures and distances in Figure 2. Here, red points represent the transverse distribution of energy density, and colored lines express the fitting curves. The left side plots show the temperature dependence at R=4a. The fitting curves and chi-squares of these plots likely show that the equation (9) is the best for small distances, R < 0.8 fm. However, from the right plots at R=10a, we can see that the equation (9)

Vol. 60 No 04 (236) 2020
DOI: https://doi.org/10.5564/pmas.v60i4.1501

is not the best choice for long distances, R>0.8fm. The curves and their chi-squares show that all fit functions can be used for long distance fittings because their chi-squares are almost equal. Therefore, we need more information to choose the fit function for long distances.

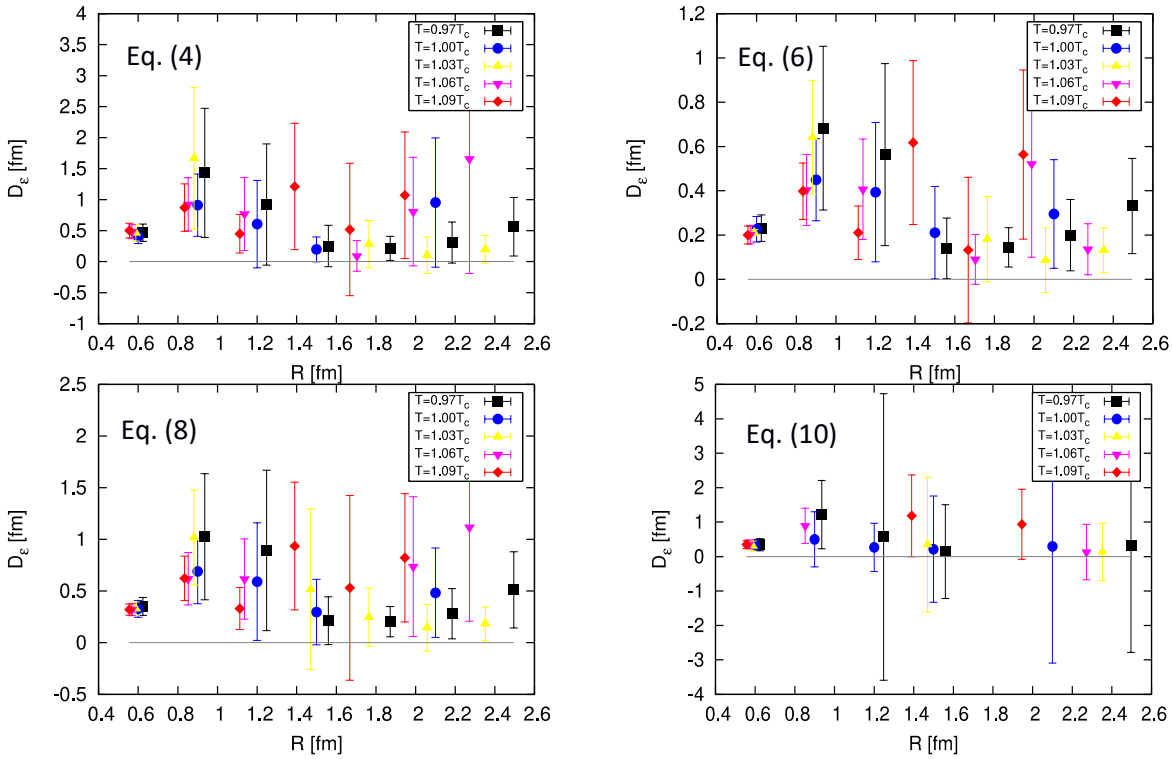

Figure 3. The widths of the flux tube as a function of the distance at four different fittings

Figure 3 depicts the physical widths of the flux tube as a function of the distance at four different fit functions. The figure shows that the width increases with the distance R until R = 1fm, then it decreases to zero. Below the critical temperature, the width rises again gradually when R > 1.5 fm. Above the critical temperature, the statistical error of the width became unacceptably large, but some data points, yellow points, can reveal that the width declines to zero with the distance until it reaches 2.6 fm. Also, we have seen that the first three fitting functions, exponential, Gaussian, and Coulombic are more suitable with the energy density data since they have computed more values of the width. Nevertheless, from Tables 1-4, the chi-square value of the Gaussian fits are mostly smaller than others where R > 0.8 fm. Also, the plot, which is determined by Gaussian function, has smaller statistical error bars than others. Consequently, we have preferred Gaussian fit for long distances.

Vol. 60 No 04 (236) 2020
DOI: https://doi.org/10.5564/pmas.v60i4.1501

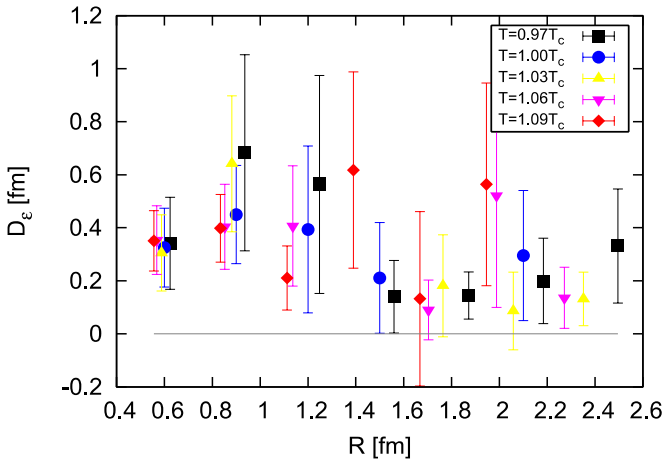

Figure 4. The final results of the fitting.

Finally, we have concluded that the four coefficient functions and the Gaussian function provide good and effective descriptions of our data. Now, let us consider the ultimate results of the fit in Figure 4. Figure 4 shows physical width of the flux tube as a function of R. Here for all temperatures, the physical width is rising with the distance until it reaches around 1 fm, after which it is decreases with a further increase in distances. The widening of the flux tube showed hadronization, besides contraction of the flux tube expressed the localization of the QCD string. The width is the increasing again slowly when R > 1.5 fm below the critical temperature. Perhaps, this is indicative of re-hadronization. Some values of the width above the critical temperature are still declining with the distance until it reaches 2.6 fm. But, we cannot find string breaking up to around R = 2.6 fm in the deconfinement phase.

CONCLUSIONS

In the present paper, we have defined suitable fit functions for the flux tube with dynamical fermions. In order to accomplish such a result, middle transverse profile of the energy density had been fitted by four different functions. We have seen that one function cannot determine the width of the flux tube through our considered temperatures and distances. Therefore, two functions were chosen in the two different distance regions, the four coefficient functions where R < 0.8 fm and the Gaussian function where R > 0.8 fm.

From the ultimate results of the width, we have seen that there is no string breaking until the distance reaches 2.6fm above the critical temperature. Also the result may point to some indication of the generation of new quarks and anti-quark pair below the critical temperature.

REFERENCES

1. S. Chagdaa, E. Galsandorj, B. Purev, O. Kaczmarek and H.T. Ding, Flux tube with dynamical fermions from high temperature SU(3) lattice gauge theory, Volume 363 - 37th International Symposium on Lattice Field Theory (2019).
2. M. Fukugita and T. Niuya, Phys. Lett. 132B, (1983) p. 374.
3. R. Sommer, Scaling of SU(2) flux distribution and potential, Nucl. Phys. B306, (1988), pp. 181-198.
4. C. Schlichter, G. S. Bali, K. Schilling, Color flux profiles in SU(2) lattice gauge theory, Nucl. Phys. B, Volume 42, Issues 1–3, (1995), pp. 273-275.
5. N. Cardoso, M. Cardoso, P. Bicudo, Inside the SU(3) quark-antiquark QCD flux tube: screening versus quantum widening, Phys. Rev. D 88 (2013) 054504, arXiv:1302.3633 [hep-lat].
6. P. Cea, L. Cosmai, F. Cuteri, and A. Papa, QCD flux tubes across the deconfinement

Vol. 60 No 04 (236) 2020
DOI: https://doi.org/10.5564/pmas.v60i4.1501

phase transition, EPJ Web of Conferences. (2017), p. 175.
7. M. Lüscher, Properties and uses of the Wilson flow in lattice QCD, JHEP 08 (2010) 071, [arXiv:hep-lat/1006.4518].
8. L. Mazur, Applications of the Gradient flow method in lattice QCD, Master's thesis, Bielefeld University (2017).